Energetic Macroscopic Representation of an Islanded Switched Reluctance Generator-based DC microgrid

Qihao Guo, Anatole Desreveaux, Demba Diallo, Imen Bahri

Université Paris-Saclay, CentraleSupélec, CNRS, Laboratoire de Génie Electrique et Electronique de Paris, 91192, Gif-sur-Yvette, France.

Sorbonne Université, CNRS, Laboratoire de Génie Electrique et Electronique de Paris, 75252, Paris, France

ABSTRACT – Switched Reluctance Generator (SRG) is a sustainable and low-cost solution for future small-scale Wind-Energy-Conversion System (WECS). However, the SRG has intrinsic spatial and magnetic nonlinearities and study of WECS is multidisciplinary and complex. To simplify the modelling and controller design process, this paper proposes a comprehensive step-by-step design method for an SRG based DC microgrid. Thanks to the Energetic Macroscopic Representation, a natural decomposition of the studied WECS with respect to physical laws is obtained. Moreover, a control scheme is easily deduced from this description using inversion-based rules. Three operating modes are evaluated: maximum power tracking, direct power control, and output voltage control. The effectiveness of the methodology is validated under variable-speed wind conditions by simulation in MATLAB/Simulink environment.

Keywords—Microgrid, Switched Reluctance Generator, Modelling, Energetic Macroscopic Representation.

Nomenclature

MPPT: Maximum Power Point Tracking

SRG: Switched Reluctance Generator

SRM: Switched Reluctance Machine

BESS: Battery Energy Storage System

MG: Microgrid

EMR: Energy Macroscopic Representation

DPC: Direct Power Control

SoC: State of Charge

AHBC: Asymmetric Half Bridge Converter

1. INTRODUCTION

The use of rare-earth materials, such as Neodymium Iron Boron, in electrical machines for wind generation applications has raised concerns in many areas. The extraction and refinement of rare earths is a potentially environmentally damaging process, resulting in sustainability problems. Political constraints can significantly influence the availability and price of rare earth materials, given the heavy reliance on a single supplier for mass production [1].

The Switched Reluctance Machine (SRM) is a sustainable and permanent magnet-free machine solution for future power generation systems in applications like small-scale wind generation systems, more-electric-aircrafts, hybrid electric vehicles, flywheel-based energy storage systems, etc [2]. This unique characteristic offers attractions in terms of motor cost and environmental footprint since the extraction and refinement of rare earth material is both an expensive and potentially environmentally damaging process. Due to its simple structure, robustness, and fault tolerance, it is very suitable for operating in conditions where reliability and economic factors are important.

A SRG-based microgrid (MG), as shown in Fig. 1, is a promising low-cost sustainable solution to maximise the utilisation of intermittent wind energies in rural areas. The establishment and control for a SRG-based DC MG is firstly presented in [3], and the power circuit components are appropriately designed to optimise the system's performance. Although this research proposed a unified voltage controller design approach, the dynamic of the wind turbines has been ignored. In [4], the DC output voltage control problem of a SRG supplying a constant power load is investigated using passivity-based control. However, the proposed method has a more complex structure than traditional linear controllers, resulting in difficulties in practical implementations. The control strategy of a SRG driven by a variable-speed wind turbine is researched in [5] and the system's performance is tested over the whole speed range. However, the maximum power point tracking (MPPT) algorithm is not clarified. The optimal combination of control variables for SRG are obtained by analysing the DC MG's energy conversion process in [6], but the speed of the wind turbine is considered as a constant value, which is not valid in real applications.

In these studies, only one operating mode, such as MPPT, is considered [7], and other operating modes of SRG are either ignored [3] or not detailed [4]. In fact, several operating modes exist according to the physical constraints of MG, such as the power balance constraint and limitation of battery's SoC. In addition, the variable-speed dynamics of wind turbines are not considered. In fact, the characteristics of wind turbine can influence the system's performance. Besides, the SRG-based DC MG is a multi-timescale system that consists of several subsystems with different dynamics. As a result, the modelling and controller design of SRG-based DC microgrid is a relatively complex process. If the controllers are not tuned appropriately, the system's performance may degrade significantly, even causing instability.

For these reasons, it is essential to propose a unified approach for systematic modelling and appropriate controller design of

SRG-based DC MG considering different operating modes. This paper applies the Energetic Macroscopic Representation (EMR) formalism [8] to simplify the modelling and controller design process. The EMR has been used in several applications such as microgrid [9] and wind turbines [10]. However, to the knowledge of the authors, there is no application of the EMR to a SRG-based DC MG that is discussed in this work. The main contributions of this research can be summarised as follows:

1) An islanded MG structure with SRG-based wind generation system is proposed.
2) The organisation of the system and controllers design using the EMR formalism.
3) Three different operating modes of SRG are proposed according to the state of the MG.

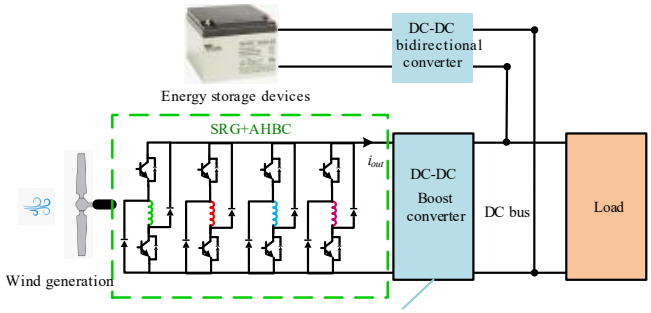

Fig. 1 The structure of SRG-based islanded DC MG

2. System Modelling and EMR

Fig. 1 presents the proposed structure of the islanded SRG-based DC MG. A battery energy storage system is applied to establish the 48V DC bus by a bidirectional DC-DC converter, which is out of scope in this paper. The SRG-based wind generation system with its Asymmetric Half Bridge Converter (AHBC) is connected to the DC bus with a boost converter. In normal operation mode, the boost converter regulates the output voltage of SRG to its nominal value of 24V. The global system can be divided into several subsystems:

- variable-speed wind turbine subsystem
- switched reluctance machine subsystem
- boost converter subsystem

The modelling of the systems will be firstly presented. Thanks to the EMR, the control scheme can be easily deduced.

2.1.1. Variable-Speed Wind Turbine

In this research, the "Piggott" type wind turbine is used [11]. It is a kind of small-scale wind turbine widely used in many off-grid and rural communities where access to electricity is a challenge. It is known for its simplicity and affordability since its rotor and blades are usually hand-carved from wood.

The mechanical power produced by a Piggott wind turbine can be expressed as

$$P_m = \frac{1}{2} C_p(\lambda, \beta) \rho S V_w^3 \qquad (1)$$

where $C_p(\lambda, \beta)$ is the power coefficient, V_w the wind velocity in m/s, β the blade pitch angle, ρ the air density, $S = \pi R^2$, where R is the radius of turbine blades. The tip-speed ratio λ is defined as:

$$\lambda = \frac{R\Omega_m}{V_w} \qquad (2)$$

,and Ω_m the rotational speed of the wind turbine. The pitch angle β can be used as a control parameter to adjust the output power in large wind turbine applications. For Piggott wind turbine, β is supposed to be 0. The mechanical torque T_m imposed on blades can be calculated as:

$$T_m = \frac{P_m}{\Omega_m} = \frac{C_p(\lambda, \beta) \rho S R^3 {\Omega_m}^2}{2\lambda^3} \qquad (3)$$

The power coefficient $C_p(\lambda, \beta)$ for Piggott wind turbine is given in Fig. 2 (a) and the mechanical torque T_m imposed on the blades as a function of wind speed is given in Fig. 2 (b) [11].

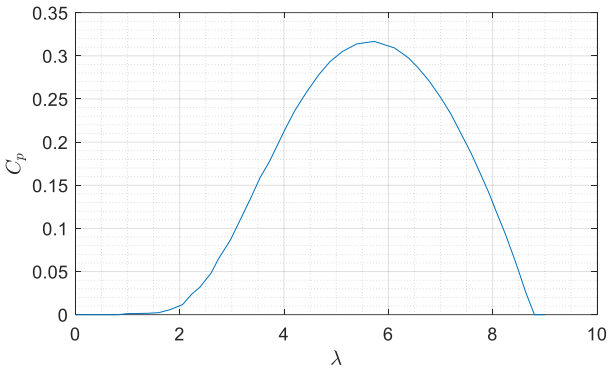

(a)

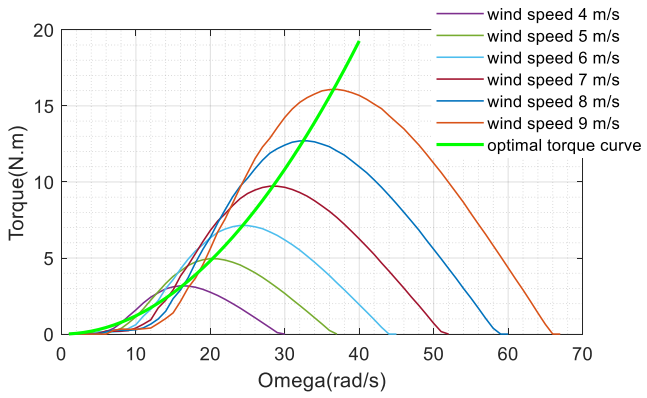

(b)

Fig. 2 Characteristics of "Piggott" wind turbine

Each wind speed has an optimal operating point where the wind turbine can output the maximum mechanical power. To maximise the power generation despite wind variations, the following electrical load torque should be imposed [12]:

$$T_{opt} = K_{opt} \Omega_m^2 \qquad (4)$$

In the above discussion, it is assumed that the characteristics of the wind turbine are known; in this case, the optimal torque reference can be easily calculated based on the rotation speed, as presented in Fig. 2 (b) (solid green line).

2.1.2. Mechanical dynamics

The mechanical dynamics of the model can be described by:

$$J \frac{d\Omega_m}{dt} + F\Omega_m = T_m + T_{e\_total}, \qquad (5)$$

where J is the total inertia of the machine and blades, F is the friction coefficient, and T_{e_total} is the SRG's total electromagnetic torque. T_{e_total} is negative in generation mode.

2.1.3. *Switched Reluctance Generator*

This paper considers the double salient 8/6 four phases SRG mentioned in [6]. The stator has eight salient poles with concentrated field coils, and the rotor is made of ferromagnetic material with six passive salient poles.

In generator mode, the electrical power is produced when the inductance decreases $\frac{dL_j(\theta,i_j)}{d\theta} < 0$, which means that the machine produces a negative torque, as shown in (8).

Fig. 3 shows the ideal inductance profile and one-phase current waveform when the hysteresis controller regulates the phase current.

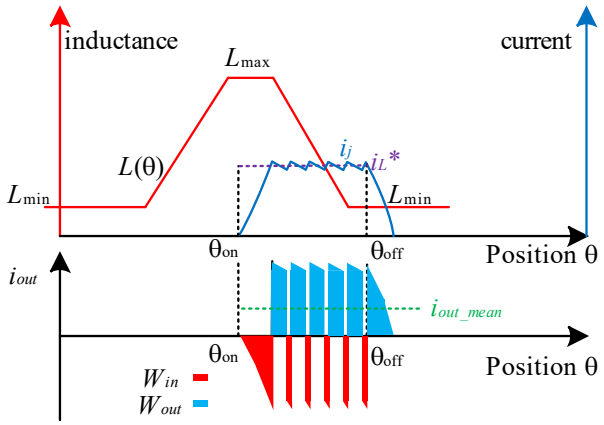

Fig. 3 The ideal inductance profile and phase current waveforms

Before making the derivation, some basic assumptions are made: 1) the nonlinear magnetic saturation and mutual coupling between phases are ignored, so each phase of the machine is assumed to be independent; 2) the mechanical losses are neglected.

The total electromagnetic torque T_{e_total} of the SRG is produced by the four phases as follows:

$$T_{e\_total} = T_e(\theta, i_1, i_2, i_3, i_4) = \sum_{j=1}^{4} T_e(\theta, i_j) \tag{6}$$

Where θ is the rotor position, and i_j the current in phase j.

Considering the intrinsic nonlinear characteristics of the SRG, a polynomial function is used to describe the relationship between T_{e_total} and $i_{total} = \sum_{j=1}^{4} i_j$, as:

$$T_{e\_total} = f_{poly}(i_{total}) \tag{7}$$

Where f_{poly} is a third-order polynomial function[13].

The electromechanical conversion in the phase j can be expressed as:

$$\begin{cases} e_j = i_j \Omega_m \dfrac{dL_j(\theta, i_j)}{d\theta}, \\ T_e(\theta, i_j) = \dfrac{1}{2} {i_j}^2 \dfrac{dL_j(\theta, i_j)}{d\theta} \end{cases} \tag{8}$$

where e_j is the back-electromotive force (EMF), $L_j(\theta, i_j)$ is known as apparent inductance [14].

The electrical dynamic equation in phase j can be expressed as:

$$v_j = r i_j + l_j(\theta, i_j) \frac{di_j}{dt} + i_j \Omega_m \frac{dL_j(\theta, i_j)}{d\theta}, \tag{9}$$

Where v_j is the terminal voltage , r the winding resistance, and $l_j(\theta, i_j)$ the incremental inductance[14].

2.1.4. *Assymetric Half Bride Converter (AHBC)*

The average model of the AHBC can be represented as:

$$\begin{cases} v_j = m_j v_{SRG} \\ i_{out} = -\sum_{j=1}^{4} \dfrac{i_j}{m_j} \end{cases} \tag{10}$$

Where v_{SRG} is the SRG output voltage, i_{out} the output current, and $m_j = \{1, -1\}$ is the control input of the AHBC for phase j.

2.1.5. *Boost Converter Subsystem Modelling*

The SRG requires a source of excitation to generate electrical energy. The SRG power generation can be separated into excitation and demagnetisation stages, as shown in Fig. 3. The difference between W_{in} the power consumed during the excitation step and W_{out} the power generated during demagnetisation is the average output power in one generation cycle.

The DC-DC boost converter is used to stabilise the terminal voltage of SRG to its nominal value of 24V, which can be regarded as the source of excitation. The average large-signal dynamics of the boost converter derived in [15], are described as:

$$C_w \frac{dv_{SRG}}{dt} = i_{out} - i_{L_w} \tag{11}$$

$$L_w \frac{di_{L_w}}{dt} + r_w i_{L_w} = v_{SRG} - v_s \tag{12}$$

$$\begin{cases} v_s = (1-d) v_{bus} \\ i_{L_w} = \dfrac{i_{bus}}{(1-d)} \end{cases} \tag{13}$$

Where the duty cycle $d(t) \in [0,1]$ is the control input, L_w and r_w are inductance filter and resistance, i_{L_w} is the inductance current, $v_{bus} = 48V$ is the DC bus voltage, C_w is the capacitance on the SRG side, v_s is the average voltage across the power switch, and i_{bus} is the DC bus current.

2.1.6. *EMR of the islanded SRG based microgrid*

Energetic Macroscopic Representation is used to organize the model of the system. EMR has been widely used since 2000 for various systems. Its advantages are a clear energy representation of systems, an easy and rapid modification of the system by adding and removing blocks, and a systematic deduction of the control scheme.

Each component of the microgrid is translated into EMR elements according to its modelling principle [8]. The EMR of the whole system is given by the upper part of Fig. 4.

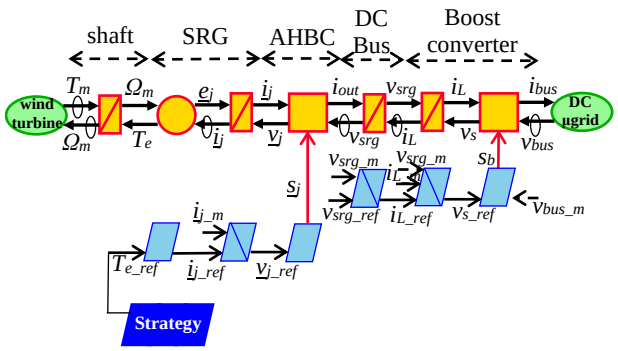

Fig. 4 EMR of the SRG-based microgrid

3. DESIGN OF THE CONTROLLERS

3.1.1. SRG averaged torque control

As for the torque control strategy, the average torque control is chosen thanks to its applicability in the whole torque-speed reference frame, and weak dependency to rotor position [16], [17].

A direct inversion of electromechanical conversion is achieved based on (7):

$$i_{j\_ref} = {f_{poly}}^{-1}(T_{e\_ref}) \tag{14}$$

3.1.2. SRG phase current control

The inversion of the SRG's phase winding (9) requires a closed-loop control to obtain v_{j_ref} from the reference current and its actual value in phase j. SRG has both spatial and magnetic nonlinearities, since the incremental inductance depends on rotor position and phase current. Besides, the EMF e_j is also nonlinear making its estimation tricky. Therefore, the traditional linear controller, such as a PI controller [18], may fail to regulate the phase current. In the following, the hysteresis current controller [19] is used thanks to its easy implementation.

$$v_{j\_ref} = Hysteresis(i_{j\_ref} - i_{j\_meas}) \tag{15}$$

3.1.3. Boost converter inductance current control

The inversion of the DC-DC boost converter model is directly achieved by an inversion of (13) as follows:

$$d_{\_ref} = 1 - \frac{v_{s\_ref}}{v_{bus}} \tag{16}$$

The inversion of the inductance current (12) requires a closed-loop control to obtain v_{s_ref} from the reference current and its actual value :

$$\begin{aligned} v_{s\_ref} = -(&K_{p\_current}(i_{L\_ref} - i_{L\_meas}) \\ &+ K_{i\_current}\int (i_{L\_ref} \\ &- i_{L\_meas})\,dt - v_{SRG}) \end{aligned} \tag{17}$$

3.1.4. Boost converter output voltage control

The inversion of the capacitance voltage (11) requires a closed-loop control to obtain i_{L_ref} from the reference voltage and its actual value. To ensure the stability of the control strategy, the dynamics of the inner inductance current control loop should be set much faster (at least 10 times) than the ones of the outer voltage loop.

$$\begin{aligned} i_{L\_ref} = -(&K_{p\_voltage}(v_{SRG\_ref} \\ &- v_{SRG\_meas}) \\ &+ K_{i\_voltage}(v_{SRG\_ref} \\ &- v_{SRG\_meas}) - i_{out}) \end{aligned} \tag{18}$$

4. STRATEGIES

The SRG-based small-scale wind generation system may operate under different operating conditions. This research has developed three different control strategies: MPPT, direct power control (DPC), and terminal voltage control. One of these strategies can be selected to give the reference torque given by the strategy block (Fig.4)

Mode 1: MPPT. The wind generator is expected to operate in MPPT mode to maximise the electrical power that can be extracted from the wind. The MPPT strategy, which is not in the scope of this paper, continually adjusts the electrical load according to the wind speed. The optimal torque control in [12] is adopted thanks to its simplicity. The load torque reference can be calculated directly according to the shaft rotational speed under the condition that the wind turbine data are known, which is our case (as displayed in Fig. 2).

$$T_{e\_ref} = K_{opt}\Omega_m^2 \tag{19}$$

Mode 2 : DPC. The wind generation system may also operate in direct power control mode to protect the BESS from overcharging, and ensure power balance in the MG. This operating mode is enabled when the required load power is less than the wind power and the SoC of the BESS reaches its maximum value. Therefore, instead of extracting the maximum power from the wind, only a part of the wind power is captured. The power reference is computed from a higher-level energy management controller, which is not in the scope of this paper.

The average output power is the product of the terminal voltage v_{SRG} and the mean value of i_{out} that is computed over a moving average window of one cycle of the fundamental frequency as follows:

$$mean(i_{out}) = \frac{1}{T}\int_t^{t+T} i_{out}\,dt \tag{20}$$

Where T = 1/fundamental frequency and the fundamental frequency is 10 Hz in this study.

The power error e_P between the reference output power P_{out_ref} and the measured output power P_{out_meas} is processed by a PI controller. The SRG's torque reference is then obtained as follows:

$$T_{e\_ref} = K_{p\_power}e_P + K_{i\_power}\int e_P\,dt \tag{21}$$

Mode 3: Terminal voltage control. In this mode, the SRG operates in self-excited mode, which means that the terminal voltage is controlled by the SRG, instead of the DC-DC boost converter. In normal operating conditions, the DC bus voltage of an islanded DC microgrid is stabilised by charging or discharging the battery energy storage system. However, if problems or malfunctions occur in the battery energy storage system, such as overcharging, overheating or physical damage, the SRG must regulate the terminal voltage.

The voltage error e_V between the reference voltage v_{SRG_ref} and the actual measured output voltage v_{SRG_meas}, is processed by a PI controller. The SRG's torque reference is then obtained as follows:

$$T_{e\_ref} = K_{p\_voltage\_srg}(v_{SRG\_ref} - v_{SRG\_meas}) + K_{i\_voltage\_srg}\int (v_{SRG\_ref} - v_{SRG\_meas})\,dt \quad (22)$$

5. Performance Evaluations by Simulation

The system models and controllers are established in MATLAB/Simulink environment.

5.1.1. *SRG terminal voltage control in normal condition*

In normal conditions, v_{SRG} the terminal voltage of the SRG is regulated to 24V by the interlinking boost converter. This terminal voltage can be regarded as a stable source of excitation to generate electrical energy. According to Fig. 5, v_{SRG} is controlled to its reference value of 24V with roughly 8% of voltage ripples.

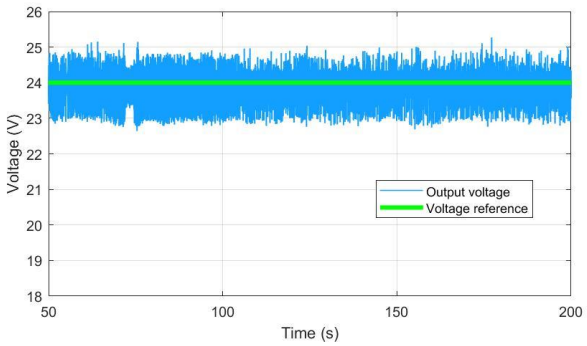

Fig. 5 The SRG terminal voltage regulation

5.1.2. *Strategy1: MPPT mode*

We use the real-time wind profile captured from French National Experimental Site for the Small Wind Farm (*Site Expérimental pour le Petit Eolien National*) to evaluate the performance of the MPPT strategy. Fig. 6 shows simulation results over 150 s. Thanks to the MPPT algorithm the produced electrical power follows the wind speed variations.

The performance of the hysteresis controller is presented in Fig. 7. The current in phase 1 (taken as an example) is well regulated. We can observe that the switching frequency is not constant due to the intrinsic feature of the hysteresis controller.

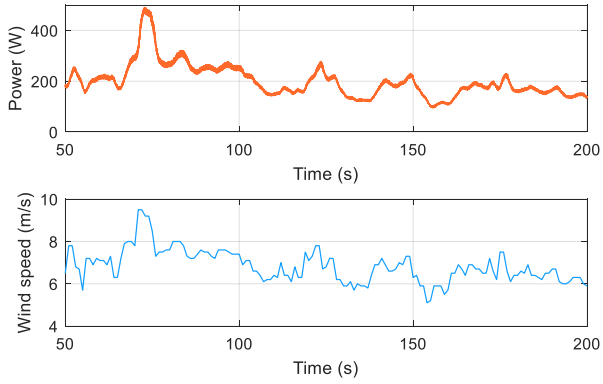

Fig. 6 Simulation results in MPPT mode

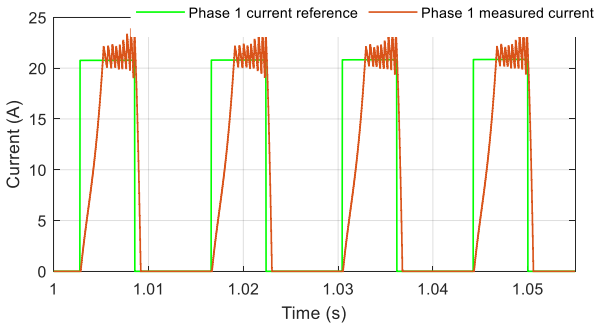

Fig. 7 Performance of the hysteresis controller for current in phase 1

5.1.3. *Strategy 2: DPC mode*

A 180-second simulation is performed to verify the performance of the DPC. The output power reference (green line) generated by a higher-level power management controller is well-tracked by the controller. The slight deviations are mainly due to variations in wind speed.

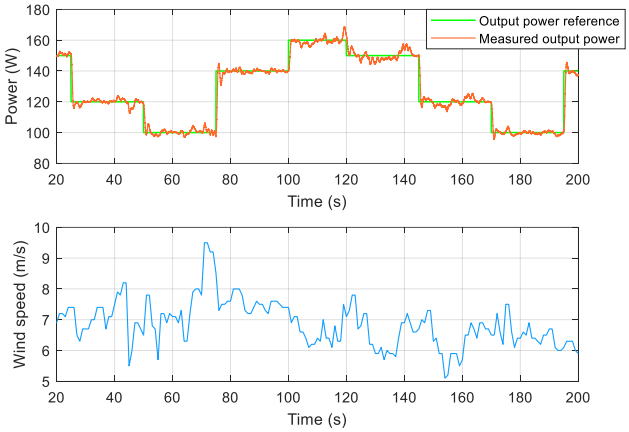

Fig. 8 Simulation results in DPC mode

5.1.4. *Strategy 3: terminal voltage control mode*

Step changes in the output voltage reference: step-up and step-down changes in the output voltage reference are introduced to evaluate the tracking capabilities. The results displayed in Fig. 9, show that the controller exhibits excellent performance in steady state and during the transients: the settling time is very short with a very small overshoot.

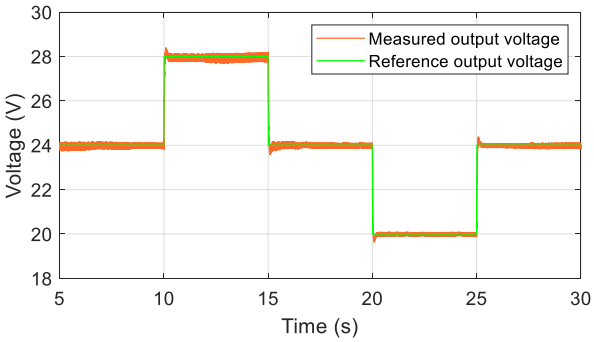

Fig. 9 Simulation results for voltage reference step changes

Load variations: Load step variations can be considered as disturbances for the voltage controller. As shown in Fig. 10, a step-down change in the load (R_{load} varies from 5 to 10 Ω at $t \approx 30.1s$). The voltage controller adjusts the electrical torque reference to its new value and the SRG produces less power to avoid any steady-state tracking error. Similarly, for a step-up

change in the load (R_{load} varies from 10 to 5 Ω at $t \approx 34.3s$), after the transient, the system settles at the new operating point and the output voltage is still equal to its reference value of 24V.

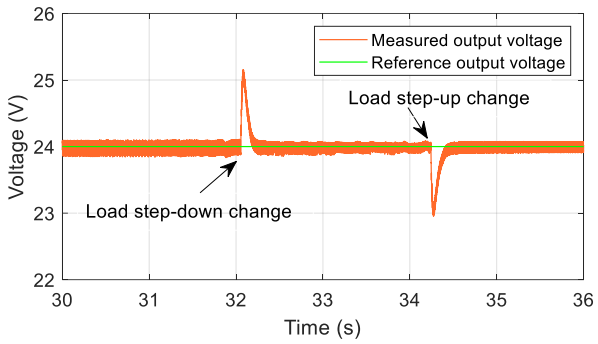

Fig. 10 Simulation results for load step changes

6. Conclusions

According to the optimisation objective and physical constraints of the MG, the performance of a SRG-based DC MG is evaluated under three different modes: MPPT, DPC and terminal voltage control. A systematic method of controller modelling and design is applied through EMR formalism. This step-by-step model-based design methodology is an aid in designing appropriate controllers with good dynamic performance for a complex multiphysics system. The simulation results confirm the feasibility of the proposed approach in an application to a SRG-based DC microgrid. Furthermore, the same methodology can also be applied to more complex conditions, for example, when the SRG will be connected to the AC grid and energy storage devices are present in the microgrid.

7. References

[1] J. D. Widmer, R. Martin, et M. Kimiabeigi, « Electric vehicle traction motors without rare earth magnets », *Sustainable Materials and Technologies*, vol. 3, p. 7-13, April 2015, doi: 10.1016/j.susmat.2015.02.001.

[2] M. A. Mueller, « Design and performance of a 20 kW, 100 rpm, switched reluctance generator for a direct drive wind energy converter », in *IEEE International Conference on Electric Machines and Drives, 2005.*, 2005, p. 56-63. doi: 10.1109/IEMDC.2005.195701.

[3] Y.-C. Chang et C.-M. Liaw, « Establishment of a Switched-Reluctance Generator-Based Common DC Microgrid System », *IEEE Transactions on Power Electronics*, vol. 26, nº 9. p. 2512-2527, 2011. doi: 10.1109/tpel.2011.2109013.

[4] M. M. Namazi, H. R. Koofigar, et J. W. Ahn, « Active Stabilization of Self-Excited Switched Reluctance Generator Supplying Constant Power Load in DC Microgrids », *IEEE Journal of Emerging and Selected Topics in Power Electronics*, vol. 9, nº 3, p. 2735-2744, June 2021, doi: 10.1109/JESTPE.2020.2994017.

[5] R. Cárdenas, R. Peña, M. Pérez, J. Clare, G. Asher, et P. Wheeler, « Control of a switched reluctance generator for variable-speed wind energy applications », *IEEE Transactions on Energy Conversion*, vol. 20, nº 4, p. 781-791, Dec. 2005, doi: 10.1109/TEC.2005.853733.

[6] A. Sarr, I. Bahri, E. Berthelot, A. Kebe, et D. Diallo, « Switched Reluctance Generator for Low Voltage DC Microgrid Operation: Experimental Validation », *Energies*, vol. 13, nº 12. 2020. doi: 10.3390/en13123032.

[7] T. A. D. S. Barros, P. J. D. S. Neto, P. S. N. Filho, A. B. Moreira, et E. R. Filho, « An Approach for Switched Reluctance Generator in a Wind Generation System with a Wide Range of Operation Speed », *IEEE Transactions on Power Electronics*, vol. 32, nº 11, p. 8277-8292, Nov. 2017, doi: 10.1109/TPEL.2017.2697822.

[8] A. Bouscayrol, P. Delarue, X. Guillaud, W. Lhomme, et B. Lemaire-Semail, « Simulation of a Wind Energy Conversion System using Energetic Macroscopic Representation », in *2012 15th International Power Electronics and Motion Control Conference (EPE/PEMC)*, Novi Sad, Serbia: IEEE, Sept. 2012, p. DS3e.8-1-DS3e.8-6. doi: 10.1109/EPEPEMC.2012.6397362.

[9] T. Yuan, X. Dong, X. Chen, W. Cao, J. Hu, et C. Liu, « Energetic macroscopic representation control method for a hybrid-source energy system including wind, hydrogen, and fuel cell », *Journal of Renewable and Sustainable Energy*, vol. 10, nº 4, p. 043308, Aug. 2018, doi: 10.1063/1.5038091.

[10] A. Bouscayrol, X. Guillaud, P. Delarue, et B. Lemaire-Semail, « Energetic Macroscopic Representation and Inversion-Based Control Illustrated on a Wind-Energy-Conversion System Using Hardware-in-the-Loop Simulation », *IEEE Transactions on Industrial Electronics*, vol. 56, nº 12, p. 4826-4835, Dec. 2009, doi: 10.1109/TIE.2009.2013251.

[11] A. Prevost, R. Delpoux, V. Lechappe, U. Lyon, I. Lyon, et U. C. B. Lyon, « Evaluation de deux stratégies de conversion AC/DC pour les éoliennes équipées de génératrices synchrones à aimants permanents », 16 ème Conférence des Jeunes Chercheurs en Génie Electrique (JCGE 2021), p. 7, Juin, 2022.

[12] A. Mirecki, X. Roboam, et F. Richardeau, « Architecture Complexity and Energy Efficiency of Small Wind Turbines », *IEEE Transactions on Industrial Electronics*, vol. 54, nº 1, p. 660-670, Feb. 2007, doi: 10.1109/TIE.2006.885456.

[13] H. Hannoun, M. Hilairet, et C. Marchand, « Design of an SRM Speed Control Strategy for a Wide Range of Operating Speeds », *IEEE Transactions on Industrial Electronics*, vol. 57, nº 9, p. 2911-2921, Sept. 2010, doi: 10.1109/TIE.2009.2038396.

[14] N. A. Demerdash et T. W. Nehl, « Electric machinery parameters and torques by current and energy perturbations from field computations. I. Theory and formulation », *IEEE Transactions on Energy Conversion*, vol. 14, nº 4, p. 1507-1513, 1999, doi: 10.1109/60.815098.

[15] Q. Guo, I. Bahri, and D. Diallo, « A Comparative Study of Two Control Strategies for DC-DC Boost Converter Used in DC Microgrids », in *IECON 2021 – 47th Annual Conference of the IEEE Industrial Electronics Society*, oct. 2021, p. 1-6. doi: 10.1109/IECON48115.2021.9589824.

[16] H. Hannoun, « Etude et mise en oeuvre de lois de commande de la machine à réluctance variable à double saillance », Thèse de doctorat, Paris 11, 2008. Consulté le: 20 avril 2022. [En ligne]. Disponible sur: http://www.theses.fr/2008PA112199

[17] A. Sarr, « Amélioration de la sûreté de fonctionnement d'un actionneur électrique à réluctance variable », Thèse de doctorat , Université Paris Saclay (COmUE), 2018. Consulté le: 22 février 2022. [En ligne]. Disponible sur: https://tel.archives-ouvertes.fr/tel-02145225

[18] M. Zhang, I. Bahri, X. Mininger, C. Vlad, et E. Berthelot, « Vibration Reduction Control of Switched Reluctance Machine », *IEEE Transactions on Energy Conversion*, vol. 34, nº 3, p. 1380-1390, Sept. 2019, doi: 10.1109/TEC.2019.2908458.

[19] G. Fang, F. Pinarello Scalcon, D. Xiao, R. Vieira, H. Grundling, et A. Emadi, « Advanced Control of Switched Reluctance Motors (SRMs): A Review on Current Regulation, Torque Control and Vibration Suppression », *IEEE Open Journal of the Industrial Electronics Society*, vol. 2, p. 280-301, April 2021, doi: 10.1109/OJIES.2021.3076807.